High-pressure Raman scattering and x-ray diffraction of the relaxor ferroelectric $0.96Pb(Zn_{1/3}Nb_{2/3})O_3$-$0.04PbTiO_3$

Muhtar Ahart,[1] Ronald E. Cohen,[1] Viktor Struzhkin,[1] Eugene Gregoryanz,[1] Daniel Rytz,[2] Sergey A. Prosandeev,[3] Ho-kwang Mao,[1] and Russell J. Hemley[1]

[1]*Carnegie Institution of Washington, 5251 Broad Branch Road, NW, Washington, D.C. 20015, USA*

[2]*F. E. E. Gmbh, Struthstrasse 2, D-55743 Idar-Oberstein, Germany*

[3]*National Institute of Standards and Technology, Gaithersburg, Maryland 20899-8520, USA*

(Received 11 October 2004; published 1 April 2005)

High-pressure Raman scattering and x-ray diffraction of lead zinc niobate-lead titanate (PZN-4%PT) solid solution were measured from ambient pressure to 13 GPa. All of the Raman peaks are broad due to the disorder of Zn^{2+} and Nb^{5+} on the *B* site of the perovskite structure. The pressure shifts of the Raman bands are reversible, and no pressure-induced soft phonon modes were found. X-ray diffraction as a function of pressure revealed diffuse scattering near the Bragg peaks, and gave a bulk modulus of 111 GPa assuming $K'=4$. Allowing K' to vary gave a large value $K'=12$ and $K_0=90$ GPa. Changes in both the Raman spectra and the diffuse scattering reflect suppression of the local distortions in the material on compression.

DOI: 10.1103/PhysRevB.71.144102 PACS number(s): 77.84.−s, 62.50.+p, 78.30.−j, 61.10.Nz

I. INTRODUCTION

Lead-based relaxor materials with complex perovskite structures such as $PbMg_{1/3}Nb_{2/3}O_3$-$PbTiO_3$ and $PbZn_{1/3}Nb_{2/3}O_3$-$PbTiO_3$ are characterized by broad and frequency dispersive dielectric maxima. They are of great interest not only from the standpoint of applications but also because of the fundamental questions that they present. These materials have very high electromechanical coupling coefficients ($k_{33}>90\%$) and very high piezoelectric constants ($d_{33}>2000$ pC/N).[1–5] These values are much larger than those of $PZr_xTi_{1-x}O_3$, for example, and are therefore very promising for applications as transducers, high performance solid-state actuators, and for use in ultrasonic imaging devices. A variety of theoretical approaches have been used to explain the intriguing properties of relaxor ferroelectrics, including superparaelectric,[6] dipolar glass,[7] spherical random-bond-random field,[8] domain-type dynamics,[9] and random-field-induced domain states[10] models. The ease of polarization rotation[11] in relaxors underlies their complex behavior. The presence of polar nanoscale regions (PNR) up to the Burns temperature T_B (Ref. 12) and their interactions are generally believed to be responsible for relaxor behavior, but their microscopic nature of these regions remains unclear. A fundamental understanding of the lattice dynamics of relaxor systems has not yet been established. High-pressure studies will help elucidate the origins of relaxor properties.

In these systems, two different cations randomly occupy the *B* site of the perovskite structure. There is both chemical and polarization disorder. The phase diagram of the solid solution PZN-*x*PT contains a rhombohedral phase for $0<x<8\%$, an intermediate phase associated with the morphotropic boundary (MPB) for $8\%<x<11\%$, and a tetragonal phase for $x>11\%$ at ambient pressure and room temperature.[13] Furthermore, one end member (PZN) is a typical relaxor and the other end member (PT) is a conventional ferroelectric material.

There have been few studies of the high-pressure behavior of relaxor ferroelectrics.[14–18] Studies done to date include high-pressure dielectric measurements on compositionally disordered ABO_3 oxides indicating that the pressure-induced ferroelectric-to-relaxor crossover is a common phenomenon and can be explained by a decrease in the correlation length between dipole moments.[14] High-pressure Raman studies of the relaxor PMN reveal broad features typical for relaxors. At 4.5 GPa, a new peak splits from a broader band centered at 270 cm^{-1} suggesting a displacive transition to a high-pressure phase.[17] High-pressure x-ray diffuse scattering of PMN reveals butterfly-shaped diffuse scattering that decreases under pressure and gradually disappears.[18] The authors suggested the existence of a high-pressure long-range ordered antiferroelectric phase with a doubled unit cell.

We have combined high-pressure Raman scattering and x-ray diffraction to study compressional effects on single crystals of PZN-4%PT. The same pressure-transmitting medium and diamond anvil cells were used for the Raman and x-ray studies to facilitate comparison. This material is of interest due its simple structure (rhombohedral *R*3*m* symmetry at ambient conditions) when compared to the MPB phases which may contain multiple coexisting phases (e.g., monoclinic, orthorhombic, and tetragonal). It also displays excellent electromechanical coupling coefficients. The composition with the largest value of electromechanical coupling coefficient is located near the MPB. Raman scattering of several compositions of PMN-*x*PT were reported[19] previously; different compositions show similar spectra, so we do not expect major differences in spectra between 3–5%PT. Unpoled crystals show typical broad, relaxorlike dispersive dielectric maxima. On cooling in an applied electric field, however, they show a sharp ferroelectric phase transition[20] and are expected to have a complex behavior.

II. EXPERIMENTAL TECHNIQUES

We employed two different setups for the Raman spectroscopy. The first was an *XY* Dilor triple grating system with the CCD to measure the spectrum from 1000 down to 20 cm^{-1}. The second was a Jobin Yvon HR-460 single grat-

 ©2005 The American Physical Society

ing system with double notch filters with higher throughout but a higher low-frequency cutoff of 80 cm^{-1}. Diamond-anvil cells (DACs) were used with a 4:1 mixture of methanol and ethanol as the pressure-transmitting medium. Additional experimental details are described elsewhere.[21] The single crystals of PZN-4%PT were grown by the flux method. The unpoled sample was a (001) plane parallel plate and the multidomain structures were visible by polarized light microscopy. Polished single crystals of PZN-4% PT (with a thickness of 30 μm and lateral dimensions of 70–120 μm) were loaded into stainless steel gaskets with small ruby chips for pressure determination. An Ar-ion laser was used as the light source, operating at the 514.5 nm wavelength with the average incident power of <0.2 W. The scattering geometry was 135°. All spectra were measured at 300 K (±1) and the average acquisition time was between 30 and 120 s. High-pressure x-ray powder diffraction was measured at Sector 16 (HPCAT) of the Advanced Photon Source (APS), Argonne National Laboratory. The ground powder samples of PZN-4%PT and a 4:1 mixture of methanol and ethanol were loaded into the same cell as the pressure medium. The beam wave length was $\lambda = 0.4028$ Å. The average acquisition time for x-ray diffraction was 10 s. Note that the same DAC and pressure media were used in both experiments in order to maintain a uniform sample environment.

III. RESULTS

Figure 1 shows the Raman spectra of single-crystal PZN-4%PT at selected pressures. The bands are broad in comparison to the first-order scattering of conventional end-member ferroelectrics, such as $PbTiO_3$, which show sharp peaks in their polar phases.[22] The frequency of the strong band at 50 cm^{-1} has a slight pressure dependence, hardening on compression. The sharp peak near the 350 cm^{-1} increases its intensity with pressure after 5 GPa. The linewidth of the band at 550 cm^{-1} also increases with pressure. To obtain additional information we normalized the measured spectra with the Bose-Einstein factor $n(\omega)+1$ where $n(\omega) = [(\exp(\hbar\omega/k_BT)-1]^{-1}$, ω is frequency, $\hbar$ is Planck's constant, k_B is the Boltzmann constant, and T is the temperature. We then decomposed the measured profiles using a multi-peak fitting procedure (Fig. 1). Reasonable results could be achieved with the assumption that peaks are described by spectral functions of damped harmonic oscillators to determine the pressure dependence of each Raman mode (Fig. 2). The fitted linewidths of the Raman peaks are shown in Fig. 3.

The observed Bragg reflections in the x-ray measurements demonstrate that PZN-4%PT adopts an average rhombohedral $R3m$ structure which is slightly distorted from the parent cubic perovskite structure ($Pm\bar{3}m$, O_h; Fig. 4). Butterfly-shaped diffuse scattering appears near the fundamental Bragg peaks (Fig. 5). We use a simple Lorentzian function $I_{\text{diffuse}} = I_0\Gamma/(\omega^2+\Gamma^2)$, to describe the average diffuse scattering, where I_0 is the integrated intensity of the diffuse scattering around the ring, ω is the scattering angle, and Γ is the half width at half maxima (Fig. 8). Average was performed around the diffraction ring. With pressure, the intensity of the diffuse scattering drastically decreases and the linewidth increases (Fig. 8, insets).

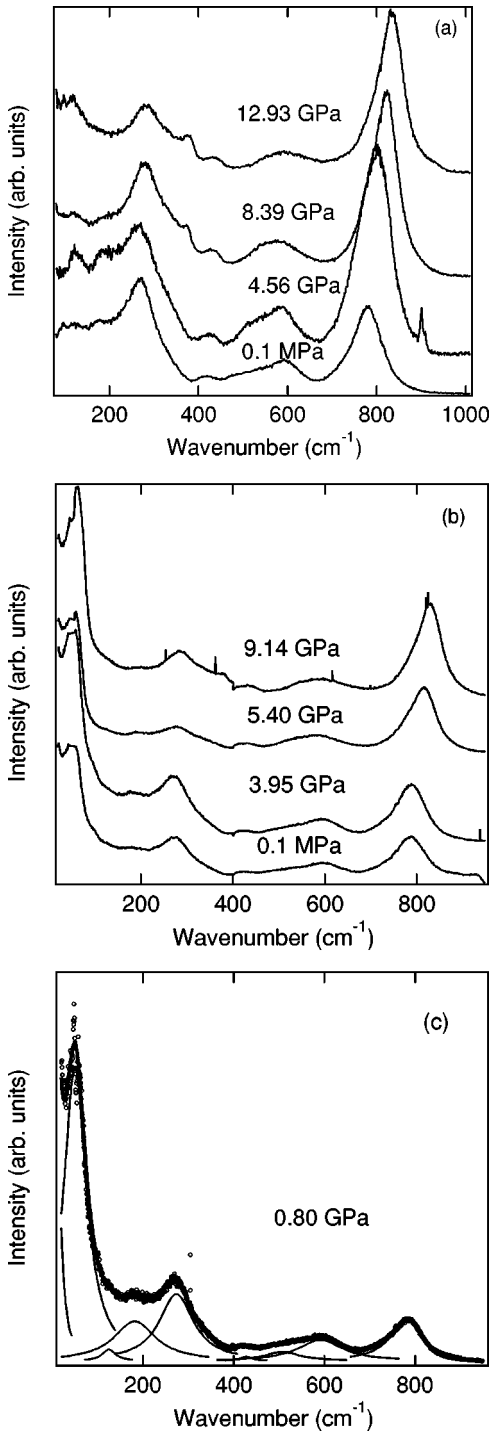

FIG. 1. Raman spectra of PZN-4%PT (uncorrected) at selected pressure. (a) Spectral range of 80–100 cm^{-1} (HR-460 single grating system). (b) Spectral range of 20–1000 cm^{-1} (*XY* Dilor triple grating system). (c) Example of a Raman spectrum normalized by the Bose-Einstein factor and fitted with multiple symmetric peaks.

The d spacings shift monotonically with pressure (Fig. 6). Figure 7 shows the pressure dependence of the (hexagonal) unit cell volumes, along with fits to a Vinet equation[23] of state $P = 3[K_0(1-x)/x^2]\exp[\frac{3}{2}(K_0'-1)(1-x)]$, where x

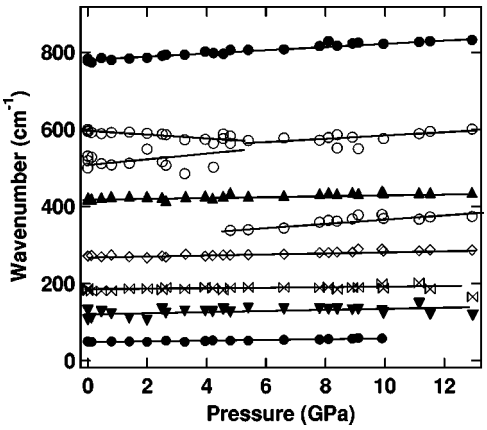

FIG. 2. The pressure dependencies of the Raman bands. The solid lines are linear fits. They are 50 cm^{-1}: $\nu=48.4(\pm0.5)+0.93(\pm0.09)P$; 130 cm^{-1}: $\nu=115.0(\pm3.8)+1.48(\pm0.38)P$; 183 cm^{-1}: $\nu=183.2)\pm0.53.3)+1.45(\pm0.69)P$; 270 cm^{-1}: $\nu=270(\pm0.8)+1.38(\pm0.09)P$; 323 cm^{-1}: $\nu=323.1(\pm0.9)+3.94(\pm0.09)P$; 422 cm^{-1}: $\nu=422.2(\pm0.7)+1.24(\pm0.07)P$; 513 cm^{-1}: $\nu=513.2(\pm1.0)+8.7(\pm0.11)P$; 595 cm^{-1}: $\nu=595(\pm1.1)-4.58(\pm0.12)P$; 553 cm^{-1}: $\nu=553.2(\pm0.8)+3.38(\pm0.09)P$; 780 cm^{-1}: $\nu=779.8(\pm1.1)+4.19(\pm0.13)P$.

$=(V/V_0)^{1/3}$, V_0 is the volume at ambient pressure, K_0 is the bulk modulus, and K_0' is bulk modulus derivative. We used the V_0 of 199.2 Å^3 at ambient pressure which is obtained by extrapolating the measured d spacings to 0.1 MPa. We performed two fits; in the first fit we assumed $K_0'=4$ (Ref. 23) and obtained $K_0=111(\pm5)$ GPa(fit A). Because the pressure-volume data show some curvature, we also fit the data with an adjustable K_0', and obtained $K_0=90(\pm5)$ GPa, and $K_0'=12(\pm3)$ (fit B).

IV. DISCUSSION

Cubic perovskites exhibit no first-order Raman scattering. The origin of the observed strong Raman scattering in perovskite relaxors may be ascribed to local chemically ordered regions or to relaxation of Raman selection rules due to disorder. Experimental evidence for locally ordered regions has been obtained from transmission electron microscopy (TEM) which indicates chemical short-range order. Specifically, 1:1 ordered domains of dimensions 50 Å are formed in these relaxors.[24] The main features of the Raman spectrum of PMN reflect $Fm\bar{3}m$ symmetry[25] are consistent with rock salt ordering. From the similarity of our material to PMN, we assume that if ordered regions in the sample have 1:1 ordering on the octahedral sites, the local structure would have $Fm\bar{3}m$ symmetry. The classification of the normal modes of 1:1 ordered $Fm\bar{3}m$ structure is $2F_{2g}+E_g+A_{1g}$. Based on previously established systematics for perovskites, we assign the band at 780 cm^{-1} to the A_{1g} mode and the broad band at 500–600 cm^{-1} to the E_g mode. The intense band at 50 cm^{-1} and the broad band at 272 cm^{-1} can be assigned to the F_{2g} modes. The remaining Raman features are more complex and cannot be explained simply using this picture. Indeed, this is evidence for lowering of symmetry from $Fm\bar{3}m$ selection rules. The polarization and chemical disorder cause vibrational modes to have coherence lengths that are small compared with their wavelengths. Such modes are not characterized by a single wave vector and will not obey momentum selection rules; all wave vectors contribute to the scattering process, causing broad features.[26,27]

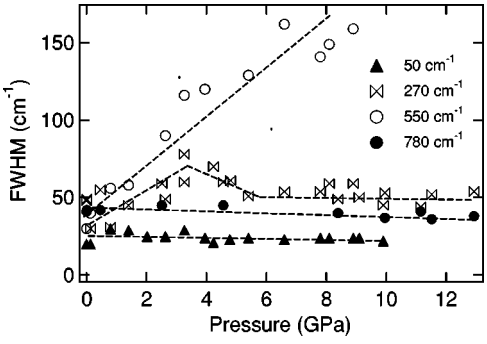

FIG. 3. The pressure dependencies of the linewidth (FWHM) of the Raman bands. The linewidths of the Raman bands at 50 (F_{2g} mode) and 780 cm^{-1} (A_{1g} mode) decrease slightly with pressure, and the linewidth of the Raman band at 270 cm^{-1} (F_{2g} mode) shows no drastic change. In contrast, the linewidth of the Raman band at 550 cm^{-1} (E_g) increases rapidly with pressure. The solid lines are the guides to the eye.

We assign the Raman bands we observe in PZN-PT by comparison with first-principles lattice dynamics for PMN (Ref. 28). The results of the polarized Raman measurements of PZN-4%PT in *VV* and *VH* geometries at room temperature are similar to the results of previous work,[29] which show that the intensity of the A_{1g} 780 cm^{-1}mode is higher by about 30% in *VV* scattering geometry below the Curie temperature. The A_{1g} band at 780 cm^{-1} is a fully symmetrical breathing vibration of oxygen octahedra. This mode slightly hardens with pressure and its linewidth decreases only slightly (Figs. 2 and 3). It is insensitive to both temperature and pressure.[28] The E_g band at 550 cm^{-1} corresponds to antiphase breathing of oxygen octahedra. The E_g mode of PMN splits into two peaks with decreasing temperature, due to tetragonal or monoclinic distortions.[28] This band shows splitting with decreasing temperature, giving two distinct peaks at low temperature (77 K),[19,30] perhaps due to greater polar distortions with deceasing temperature.[28] As expected, we find that pressure suppresses the local polar distortions. The E_g band broadens with pressure; it becomes a diffuse peak at 5 GPa (Figs. 2 and 3). This effect reflects reduced ferroelectric behavior with pressure and the formation of a paraelectriclike phase. The F_{2g} bands at 50 and 272 cm^{-1} all slightly harden with pressure. Also, a peak at 350 cm^{-1}, which overlaps with the broad band at 272 cm^{-1}, increases its intensity on compression. This effect can be explained by pressure-induced tilting of octahedra or by the appearance of F_{2g} vibrations at high pressure due to lowering of the potential barriers between multiple wells. The appearance of the F_{2g} vibration at high pressure is consistent with our explanation for the E_g mode. The pressure dependencies of the Raman spectrum indicate that polar correlations decrease with increasing pressure. This general conclusion is in good agree-

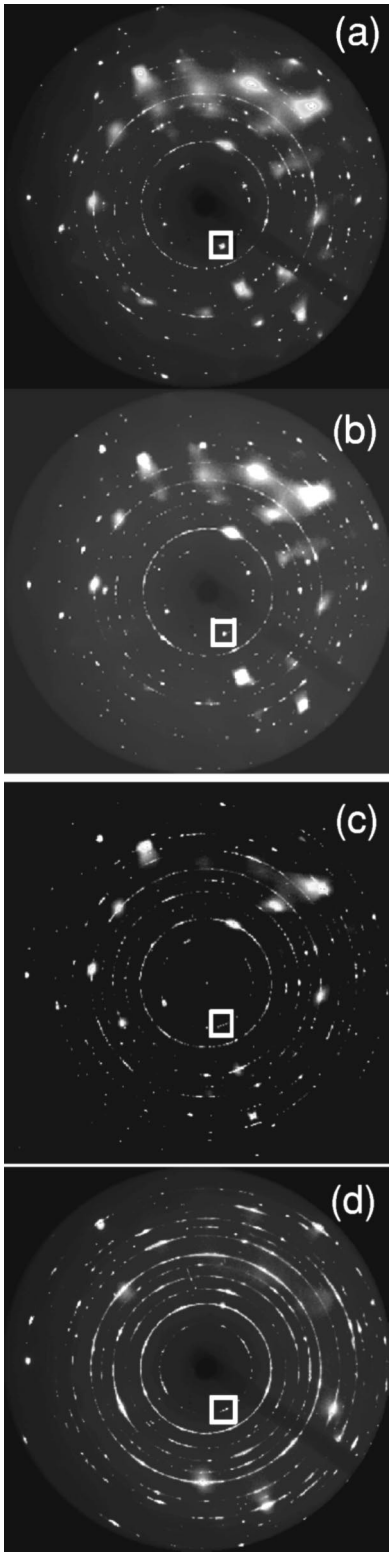

FIG. 4. X-ray diffraction patterns at selected pressures. The rings represent the Bragg reflections and the bright spots near the Bragg reflections are the diffuse scattering patterns. The white boxes show regions expanded in Fig. 5 near the 100 Bragg reflections for each image. (a) 0.3 GPa, (b) 1 GPa, (c) 4 GPa, (d) 7.7 GPa. The diffuse scattering decreases markedly with pressure.

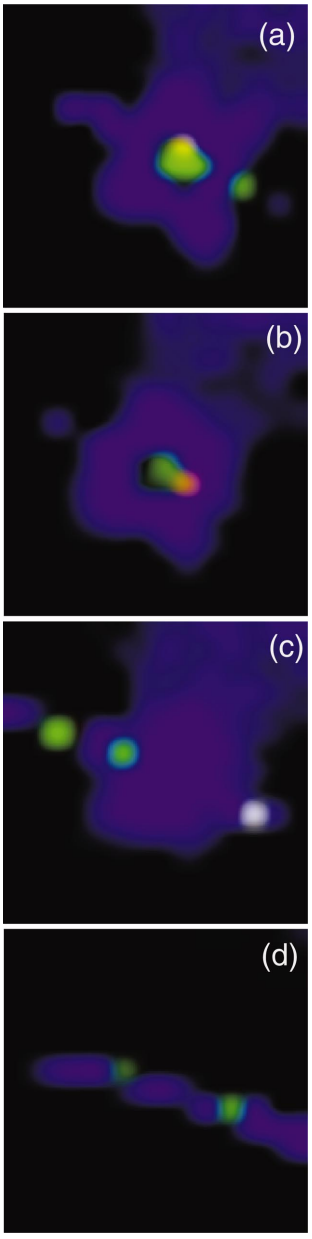

FIG. 5. (Color) Butterfly-shaped diffuse scattering near a 100 reflection at selected pressure: (a) is an enlargement of the white box region of Fig. 4(a), P=0.3 GPa, (b) is an enlargement of the white box region of Fig. 4(b), P=1 GPa, (c) is an enlargement of the white box region of Fig. 4(c), P=4 GPa, (d) is an enlargement of the white box region of Fig. 4(d), P=7.7 GPa. By 7.7 GPa, the diffuse scattering is gone.

ment with the observations of Samara *et al.*[14]

The diffuse scattering can be due to either dynamical or static disorder.[31] Dynamic diffuse scattering is due to thermal excitations, whereas static diffuse scattering is due to structural and/or chemical disorder. The temperature dependence of the diffuse scattering[32,33] of PMN indicates that the diffuse scattering goes away above the Burns Temperature (T_B); and increases in intensity with decreasing temperature below T_B. Based on this result, and we propose that thermal excitations do not represent the dominant contribution to the diffuse scattering in relaxor ferroelectric materials. If thermal exci-

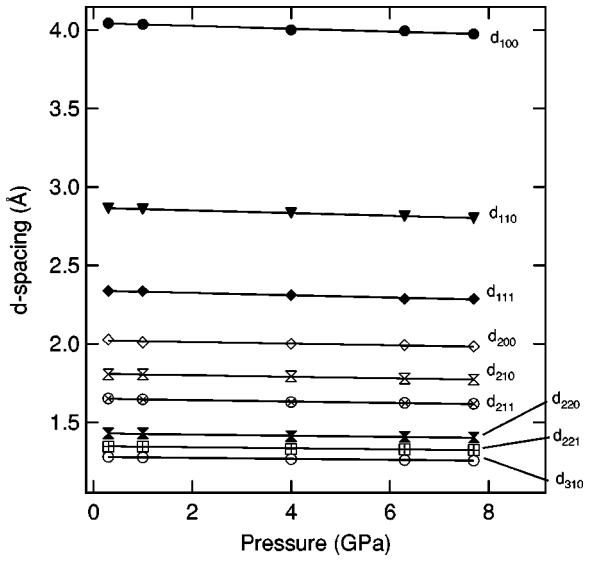

FIG. 6. *d* spacings measured and used in the volume calculations. The solid lines are the linear fits.

tations were dominant, then the diffuse scattering would increase in intensity at higher temperatures, but this was not observed. Since chemical order does not change at the Burns temperature, it seems that the diffuse scattering must be due to static polarization disorder below T_B. Further evidence against a chemical disorder origin is that pressure does not induce increased compositional fluctuations and disorder in samples of fixed compositions. There is no evidence for pressure-induced heterogeneity in the sample on pressurization. Chemical segregation would also produce x-ray diffuse scattering around the incident beam[31] which is not observed (see Fig. 4). We conclude that pressure mainly changes local polarizations and their coupling.

The diffuse scattering patterns near the Bragg peaks are asymmetric, and are evidence as discussed above for local deformations of the crystal lattice.[34] The anisotropic component of the diffuse scattering has been observed in many experiments.[32,33] In a recent study the anisotropic diffuse scattering in relaxors was suggested to be due to local ferroelectric polarization accompanied with the local microdeformation, resulting in Huang scattering.[34] The experimental and calculated intensity maps (assuming the distortion is tetragonal) are in good agreement in Ref. 34 and are similar to those observed in our measurement. This gives evidence for a Huang scattering origin of the anisotropic diffuse component. Huang scattering is produced by static elastic microdeformation in the crystal and defects.[34] Therefore, the diffuse scattering in relaxor ferroelectrics is most likely due to local ferroelectric polarizations accompanied with local microdeformation around PNR,[33,34] and the butterfly-shaped diffuse scattering pattern is evidence for tetragonal distortions[34] in local areas. It seems that local tetragonal distortions in PZN-PT must be due to the PT component, which is strongly tetragonal, except that similar diffuse scattering is observed in pure PMN. Thus it seems there must be local polar regions with (001) polarization and strain, or those regions are large enough to contain multiple $(\pm 1 \pm 11)$ type polarizations that sum to a tetragonal polarization with attendant tetragonal strain.

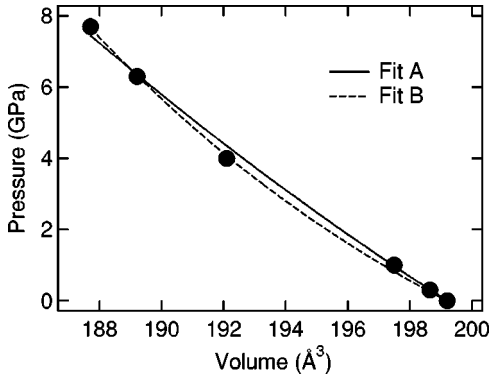

FIG. 7. The pressure dependence of hexagonal unit cell volume of PZN-4%PT. The lines are the Vinet equation of state fits. Fit A is V_0=199.2 Å^3, K_0=111(±5) GPa, and assumed K_0'=4 and fit B is V_0=199.2 Å^3, K_0=90(±5)GPa, and K_0'=12(±)3.

The decrease in intensity of the x-ray diffuse scattering with pressure is consistent with the results of earlier observations on PMN (Ref. 18). The disappearance of diffuse scattering at 5 GPa is further evidence of loss of polarization at high pressure. The reciprocal lattice points near which the diffuse scattering is observed provide information about the internal structure of the regions. The width Γ of the diffuse scattering gives us an idea about the spatial extension of these regions in different directions and their orientation.[34] Based on the experimental results, we can qualitatively estimate that the polarization and the distortions in local regions decreased by about 70% with pressure (Fig. 8) from ambient to 7.7 GPa. On compression, the tetragonal distortion is suppressed and disappears at 5 GPa. The results are fully consistent with the Raman data, which also indicate a suppression of the tetragonal distortion on compression.

Polarization rotation from $\langle 111 \rangle$ in the rhombohedral phase to $\langle 001 \rangle$ in the tetragonal phase in an applied electric field has been suggested as an explanation for the giant piezoelectric response in single crystals of PZN-PT and PMN-PT (Ref. 11). Our experimental results provide insight into this proposition. Assuming the ferroelectric mode potentials are randomly distributed in relaxor ferroelectrics, each cation (or rather local mode) occupies a certain ferroelectric potential well. The polarization associated with the ferroelectric potential dynamically and spatially rotates under ambient conditions. If an electric field is applied, most polarizations tend to align along the external field, and at certain field strength they change their directions from rhombohedral to tetragonal directions. On compression, however, the potential barriers between the wells are lowered. At the same time the magnitude of the local polarizations decreases, leading to decreased polarization correlations. The rotational character of the polar modes becomes vibrational and finally an anharmonic vibrational character with increasing pressure. At pressures above 5 GPa, the local potentials become randomly distributed anharmonic single well potentials.

V. CONCLUSION

We have presented observations of diffuse scattering vs pressure in PZN-4%PT and measured *in situ* Raman scatter-

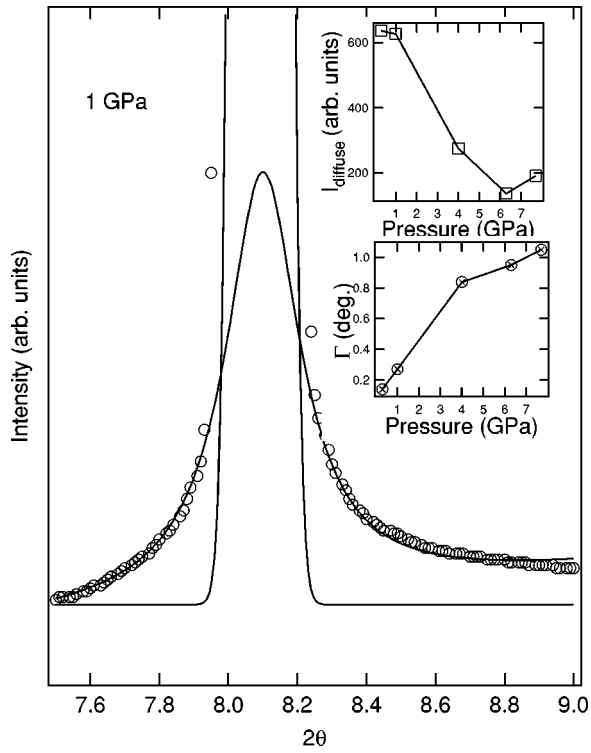

FIG. 8. The 110 reflection at 1 GPa. The wings represent the diffuse scattering integrated around the powder diffraction ring (Bragg reflection). The integrated Bragg reflections with the wings are fitted by one Gaussian and one Lorentzian functions. The upper inset represents the intensity of diffuse scattering versus pressure; the lower inset shows the linewidth versus pressure. The diffuse scattering decreases drastically with pressure.

ing under the same condition. Significant changes in the Raman spectra and x-ray diffraction pattern have been documented; high-pressure Raman scattering of the relaxor ferroelectric PZN-4%PT reveals broad bands due to disorder in the lattice. The results can be understood from the group theoretical analysis of the spectrum assuming averaged point group of $Fm\bar{3}m$. A peak with F_{2g} symmetry at 350 cm^{-1} increases its intensity with pressure and overlaps with a broad band at 272 cm^{-1}. No obvious soft-phonon-mode feature was observed. High-pressure x-ray diffraction reveals that the diffuse x-ray scattering decreases on compression and disappears at 5 GPa.

Changes in the Raman spectrum and the diffuse x-ray scattering reflect suppression of the local distortions in the material. We observed: (a) changes in the E_g mode due to the suppression of local microdeformations on compression, (b) a new peak at 350 cm^{-1} above 5 GPa possibly induced by tilting of oxygen octahedra, (c) that the diffuse scattering in relaxors are static and due to the local ferroelectric polarizations associated with the local microdeformations, (d) the reduction in the intensity of the diffuse scattering with pressure indicating that pressure suppresses the local ferroelectric polarizations. The results are consistent with previous work on PMN (Refs. 18 and 34).

In conclusion, the results can be understood in terms of the effect of pressure on the local ferroelectric effective double well potentials in which the barriers between the wells are lowered on compression, and the reduction of the correlations between the local polarizations.

ACKNOWLEDGMENTS

We are grateful to T. Salva for help with the crystal growth. We also thank D. Olga and P. Dera for the x-ray analysis of the sample. This work was supported by the Office of Naval Research under Contract Nos. N000140210506 and N000149710052 and the Department of Energy (CDAC).

[1] S. E. Park and T. R. Shrout, J. Appl. Phys. **82**, 1804 (1997).
[2] R. Zhang, B. Jiang, and W. Cao, Appl. Phys. Lett. **82**, 787 (2003).
[3] J. Yin and W. Cao, J. Appl. Phys. **92**, 444 (2002).
[4] R. Zhang and W. Cao, Appl. Phys. Lett. **85**, 6380 (2003).
[5] R. Zhang, B. Jiang, and W. Cao, Appl. Phys. Lett. **82**, 3737 (2003).
[6] G. A. Smolensky, J. Phys. Soc. Jpn. **28**, 26 (1970).
[7] D. Viehland, S. J. Jang, L. E. Cross, and M. Wuttig, J. Appl. Phys. **68**, 2916 (1990).
[8] R. Pirc and R. Blinc, Phys. Rev. B **60**, 13 470 (1999).
[9] A. E. Glazounov, A. K. Tagantsev, and A. J. Bell, Phys. Rev. B **53**, 11 281 (1996).
[10] V. Westphal, W. Kleemann, and M. D. Glinchuk, Phys. Rev. Lett. **68**, 847 (1992).
[11] H. Fu and R. E. Cohen, Nature (London) **403**, 281 (2000).
[12] G. Burns and B. A. Scott, Solid State Commun. **13**, 423 (1973).
[13] D. La-Orauttapong, B. Noheda, Z. G. Ye, P. M. Gehring, J. Toulouse, D. E. Cox, and G. Shirane, Phys. Rev. B **65**, 144101 (2003).
[14] G. A. Samara, E. L. Venturini, and V. H. Schmidt, Phys. Rev. B **63**, 184104 (2001).
[15] N. Yasuda, H. Ohwa, J. Oohashi, K. Nomura, H. Terauchi, M. Iwata, and Y. Ishibashi, J. Phys. Soc. Jpn. **66**, 1920 (1997).
[16] J. Kreisel, A. M. Glazer, P. Bouvier, and G. Lucazeau, Phys. Rev. B **63**, 174106 (2001).
[17] J. Kreisel, B. Dkhil, P. Bouvier, and J. M. Kiat, Phys. Rev. B **65**, 172101 (2002).
[18] B. Chaabane, J. Kreisel, B. Dkhil, P. Bouvier, and M. Mezouar, Phys. Rev. Lett. **90**, 257601 (2003).
[19] H. Idink and W. B. White, J. Appl. Phys. **76**, 1789 (1994).
[20] M. Shen, J. Han, and W. Cao, Appl. Phys. Lett. **83**, 731 (2003).
[21] A. F. Goncharov and V. Struzhkin, J. Raman Spectrosc. **34**, 532 (2003).
[22] C. M. Foster, Z. Li, M. Grimsditch, S. K. Chan, and D. J. Lam, Phys. Rev. B **48**, 10 160 (1993).
[23] W. L. Stixrude, R. E. Cohen, and R. J. Hemley, Rev. Mineral. **37**, 639 (1998).

[24] H. B. Krause, J. M. Cowley, and J. Wheatley, Acta Crystallogr., Sect. A: Cryst. Phys., Diffr., Theor. Gen. Crystallogr. **35**, 1015 (1979).
[25] O. Svitelskiy, J. Toulouse, and Z. G. Ye, Phys. Rev. B **68**, 104107 (2003).
[26] R. Shuker and R. W. Gammon, Phys. Rev. Lett. **25**, 222 (1970).
[27] J. E. Smith, M. H. Brodsky, B. L. Crowder, and M. I. Nathan, Phys. Rev. Lett. **26**, 642 (1971).
[28] S. A. Prosandeev, E. Cockayne, B. P. Burton, S. Kamba, J. Petzelt, Y. Yuzyuk, R. S. Katiyar, and S. B. Vakhrushev, Phys. Rev. B **70**, 134110 (2004).
[29] F. Jiang and S. Kojima, Jpn. J. Appl. Phys., Part 1 **38**, 5128 (1999).
[30] E. Husson, L. Abello, and A. Morell, Mater. Res. Bull. **25**, 539 (1990).
[31] W. A. Wooster, *Diffuse Scattering X-Ray Reflections from Crystals* (Oxford University Press, Oxford, 1962).
[32] A. Tkachuk and H. Chen, Phys. Rev. B (to be published).
[33] G. Xu, G. Shirane, J. R. D. Copley, and P. M. Gehring, Phys. Rev. B **69**, 64 112 (2004).
[34] S. B. Vakhrushev, A. Ivanov, and J. Kulda, cond-mat/0411037 (unpublished).